On the Interaction Between Autonomous Mobility on Demand Systems and Power Distribution Networks—An Optimal Power Flow Approach

Alvaro Estandia, Maximilian Schiffer, Federico Rossi, Justin Luke, Emre Can Kara, Ram Rajagopal, and Marco Pavone

***Abstract*—In future transportation systems, the charging behavior of electric autonomous mobility on demand (AMoD) fleets, i.e., fleets of electric self-driving cars that service on-demand trip requests, will likely challenge power distribution networks (PDNs), causing overloads or voltage drops. In this article, we show that these challenges can be significantly attenuated if the PDNs' operational constraints and exogenous loads (e.g., from homes or businesses) are accounted for when operating an electric AMoD fleet. We focus on a system-level perspective, assuming full coordination between the AMoD and the PDN operators. From this single entity perspective, we assess potential coordination benefits. Specifically, we extend previous results on an optimization-based modeling approach for electric AMoD systems to jointly control an electric AMoD fleet and a series of PDNs, and analyze the benefit of coordination under load balancing constraints. For a case study of Orange County, CA, USA, we show that the coordination between the electric AMoD fleet and the PDNs eliminates 99% of the overloads and 50% of the voltage drops that the electric AMoD fleet would cause in an uncoordinated setting. Our results show that coordinating electric AMoD and PDNs can help maintain the reliability of PDNs under additional electric AMoD charging load, thus significantly mitigating or deferring the need for PDN capacity upgrades.**

***Index Terms*—Electric autonomous mobility on demand, network flow, smart grid, unbalanced optimal power flow.**

Manuscript received July 6, 2020; revised July 13, 2020 and December 19, 2020; accepted January 18, 2021. Date of publication February 12, 2021; date of current version September 17, 2021. This work was supported in part by the National Science Foundation (NSF) under the CAREER and CPS programs, in part by the Toyota Research Institute (TRI), and in part by the Stanford Bits & Watts EV50 Project. The work of Alvaro Estandia was supported by the Zeno Karl Schindler Foundation with a Master's Thesis Grant. This article solely reflects the opinions and conclusions of its authors and not NSF, TRI, any other Toyota entity, or Stanford. Recommended by Associate Editor A. Sun. *(Corresponding author: Alvaro Estandia.)*

Alvaro Estandia was with Stanford University, Stanford, CA 94035 USA. He is now with Marain Inc., Palo Alto, CA 94306 USA (e-mail: alvaro@marain.com).

Maximilian Schiffer is with the TUM School of Management,Technical University of Munich, 80333 Munich, Germany (e-mail: schiffer@tum.de).

Federico Rossi was with Stanford University, Stanford, CA 94035 USA. He is now with NASA Jet Propulsion Laboratory, California Institute of Technology, Pasadena, CA 91109 USA (e-mail: frossi2@stanford.edu).

Justin Luke and Ram Rajagopal are with the Department of Civil and Environmental Engineering,Stanford University, Stanford, CA 94035 USA (e-mail: jthluke@stanford.edu; ramr@stanford.edu).

Emre Can Kara was with SLAC National Accelerator Laboratory, Menlo Park, CA 94025, USA. He is now with eIQ Mobility, Oakland, CA 94612 USA (e-mail: eck@fastmail.com).

Marco Pavone is with the Department of Aeronautics and Astronautics, Stanford University, Stanford, CA 94035 USA (e-mail: pavone@stanford.edu).

Digital Object Identifier 10.1109/TCNS.2021.3059225

NOMENCLATURE

AMoD system

$\mathcal{A}$	Set of expanded graph arcs.
$\mathcal{A}_R$	Set of road arcs.
$\mathcal{A}_S$	Set of expanded graph arcs representing a recharging process.
$\mathcal{A}_T$	Set of expanded graph arcs representing a physical time-dependent movement in the road network.
$\mathcal{C}$	Set of discrete battery charge levels.
$c_{\mathbf{v}}$	SoC associated with expanded vertex $\mathbf{v} \in \mathcal{V}$.
$c_{v,w}$	Energy consumption for traversing road arc $(v, w) \in \mathcal{A}_R$.
$d_{v,w}$	Distance of road arc $(v, w) \in \mathcal{A}_R$.
E_c	Amount of energy in a charge level.
f_0	Network flow for rebalancing vehicles.
$\bar{f}_{v,w}$	Maximum capacity of road arc $(v, w) \in \mathcal{A}_R$.
$\bar{f}_{(v,w),t}$	Residual road capacity.
$\mathcal{M}$	Set of customer trip requests.
$\mathcal{M}_{S,\mathcal{A}_S}$	Maps a charging station s for each time step t to all arcs in $\mathcal{A}_S$ that represent charging vehicles at this station.
$\mathcal{M}_{S,\mathcal{L}}$	Maps a charging station s to the associated controllable load ℓ and distribution network d.
$\mathcal{S}$	Set of chargers in the road network.
$\bar{S}_s$	Number of charging plugs in charging station $s \in \mathcal{S}$.
$\mathcal{T}$	Set of time steps.
t_m	Departure timestep of trip request $m \in \mathcal{M}$.
$t_{\mathbf{v}}$	Time step associated with expanded vertex $\mathbf{v} \in \mathcal{V}$.
$t_{v,w}$	Time to traverse road arc $(v, w) \in \mathcal{A}_R$.
$\mathcal{V}$	Set of expanded graph vertices.

V_D Vehicle operation cost per unit distance (excluding electricity).
$V_{\mathrm{el},d}$ Price of electricity at the substation of network $d \in \mathcal{D}$.
$V_{\mathrm{el},s}$ Price of electricity in charging station $s \in \mathcal{S}$.
v_m Origin of trip request $m \in \mathcal{M}$.
$\mathcal{V}_R$ Set of road vertices.
$v_{\mathbf{v}}$ Road vertex associated with expanded vertex $\mathbf{v} \in \mathcal{V}$.
w_m Destination of trip request $m \in \mathcal{M}$.
$\delta_{C,s}$ Charging rate of charger $s \in \mathcal{S}$.
Δt Length of a time step.
λ_m Customer rate of trip request $m \in \mathcal{M}$.
$\lambda_m^{c,\mathrm{dep}}$ Number of vehicles with charge c departing to serve customer trip request m.
$\lambda_m^{t,c,\mathrm{arr}}$ Number of vehicles with charge c arriving at time t after serving customer trip request m.

OPF problem

$\mathcal{D}$ Set of distribution networks.
$\mathcal{E}$ Set of links.
$i_{n,o}^{\phi}$ Complex current through link $(n,o) \in \mathcal{E}$.
$\mathcal{L}$ Set of controllable loads.
$\mathcal{N}$ Set of buses.
n_ℓ Reference bus of controllable load $\ell \in \mathcal{L}$.
$\boldsymbol{s}_{\mathrm{con},\ell}$ Complex power of controllable load $\ell \in \mathcal{L}$.
$s_{\mathrm{inj},n}^{\phi}$ Complex power injection at phase $\phi \in \Phi_n$ in bus $n \in \mathcal{N}$.
$\boldsymbol{s}_{\mathrm{unc},n}$ Complex power of uncontrollable load in bus $n \in \mathcal{N}^+$.
v_n^{ϕ} Complex voltage at phase $\phi \in \Phi_n$ in bus $n \in \mathcal{N}$.
$\boldsymbol{Y}_n$ Shunt admittance matrix of bus $n \in \mathcal{N}$.
$\boldsymbol{Z}_{n,o}$ Impedance matrix of link $(n,o) \in \mathcal{E}$.
Φ Set of phases.

I. Introduction

FLEETS of electric self-driving cars servicing on-demand trip requests promise affordable urban mobility with 1) reduced greenhouse gas emissions [1]; 2) decreased need for parking [2]; and 3) fewer road accidents [3]. Additionally, such systems offer further benefits stemming from optimized central coordination, e.g., increased vehicle utilization compared to privately owned vehicles [2] and increased operational flexibility and efficiency compared to taxi, car-sharing, and ride-hailing services. Furthermore, electric autonomous mobility on demand (AMoD) has the potential to foster the adoption of electric vehicles (EVs) since, in a high-utilization fleet, EVs are more economical than their gasoline-powered counterparts [1]. Nonetheless, operating an electric AMoD fleet also bears inherent challenges as EVs show range limitations, which require time-consuming recharging that adds a sizable load on power distribution networks (PDNs). Studies on private EVs showed that uncoordinated charging may require costly PDN upgrades to secure stabilization, as it can destabilize PDNs due to overloads or undervoltages [4]–[6]. In contrast, we expect that intelligently coordinating the vehicles' charging would reduce such negative impacts, in particular, by reducing or deferring the need for power network upgrades.

Controlling AMoD systems entails solving a dispatching problem to assign vehicles to on-demand trip requests. The system's performance increases if empty vehicles are proactively repositioned (rebalanced) in anticipation of future demand [7]. In the past decade, multiple approaches have been presented for the control of AMoD systems with varying degrees of mathematical complexity. A first family of algorithms relies on heuristic rules to dispatch and rebalance a fleet [8], [9]. More sophisticated methods use optimization algorithms to control the AMoD system. Often, network flow models using fluidic relaxations, i.e., allowing for fractional vehicles and fractionally serviced trip requests, are used [7]. Models of this type have been extended to consider road capacities and congestion [10].

To control an *electric* AMoD system, an operator must keep track of a vehicle's state of charge (SoC) and recharge a vehicle's battery accordingly. Again, some heuristic approaches exist [11], [12]. Optimization-based algorithms are so far not amenable to large-scale problems as they rely on mixed-integer linear programs with discretized SoCs [13], [14].

At its core, the operation of an electric AMoD system induces a coupling between the power network and the transportation system. Specifically, the electric AMoD fleet represents a controllable load in time and space. All previously mentioned studies neglect the impact of an electric AMoD system on the power grid, despite the fact that even a moderate amount of EVs may significantly increase electricity prices [15] and may negatively influence the power grid's reliability [16], [17]. A few recent studies consider such a coupling *implicitly* via available capacities [18] or prices [19], but the proposed control algorithms for the electric AMoD fleet do not explicitly account for the fleet impact on the power network. Only Rossi *et al.* [20] consider the fleet impact on the power network explicitly, introducing the power-in-the-loop AMoD model, a linear model that combines a network flow model for the electric AMoD system and a balanced single-phase dc model of a *transmission* network. However, this model does not consider the PDN, which is the more appropriate grid stage to analyze mesoscopic EVs' fleet operations [21]. Notably, a single-phase dc model is not sufficient to model a PDN as it assumes a constant voltage magnitude and neglects reactive power and link resistances [22]; instead, a three-phase model is necessary [23, Ch. 1]. So far, PDNs were only considered when determining optimal charging schedules for privately owned EVs, which have to reach a certain SoC by the end of a given planning horizon [5], [6], [24] as opposed to centrally coordinated fleets. Here, an instance of the optimal power flow (OPF) problem can be solved to balance necessary charging loads with PDN-specific constraints.

In summary, individual aspects of the control problem addressed in this article, such as the control of an electric AMoD system or considering PDN models to optimally charge private EVs, have been addressed in the literature. However, to the best of our knowledge, no studies that tightly couple an electric AMoD system and PDN models currently exist.

This work addresses this gap. Specifically, our contribution is threefold. First, we present a benchmark of convex three-phase PDN power flow approximations and identify a model compatible with the characteristics of the electric AMoD problem.

We then extend the mesoscopic model in [20] to capture the operations of and interaction between an electric AMoD system and a series of unbalanced PDNs. Second, we embed this model within an optimization problem that assesses achievable benefits with respect to full cooperation between the two systems. The mesoscopic optimization's solution enables comprehensive analyses to identify bottlenecks in PDNs and inform operator decisions in the day-ahead electricity market. Third, we provide a case study of Orange County, CA, where we study the impact of an electric AMoD system on the PDNs and evaluate the benefits of coordination.

The remainder of this article is structured as follows. Section II reports the mesoscopic model for an electric AMoD system used in previous work for self-consistency. Section III surveys existing PDN models and identifies a suitable model for the electric AMoD application. Section IV discusses the interaction between the electric AMoD system and a series of PDNs. Section V details our case study of Orange County, CA and presents results that characterize the impact of electric AMoD systems on PDNs, highlighting the improvement potential stemming from coordination. Finally, Section VI concludes this article with a summary of its main findings and an outlook on future research.

II. Modeling Electric AMoD Systems

In an AMoD system, a fleet of autonomous vehicles services customer transportation requests, i.e., it picks up customers from their origin and brings them to their destination [2]. A fleet operator controls the AMoD fleet by assigning vehicles to customer requests and by routing each vehicle. Besides origin–destination trips of customers, the routing may comprise rebalancing trips in-between two customer trips as spatial and temporal mismatches between origins and destinations of different customer requests arise. In an electric AMoD problem, the fleet operator additionally controls vehicle charging schedules and rebalances vehicles based on anticipated spatial–temporal variations of vehicle SoCs and electricity prices.

We model an electric AMoD system with a network flow model as originally presented in [20], reported in this section for self-consistency. Sections III and IV then detail our main contribution by integrating this model with PDNs. To avoid integer variables, the model uses a fluidic vehicle approximation and a road graph expanded along two dimensions: 1) discrete-time and 2) vehicles' SoC.

A. General Road Network Representation

We model the road network as a graph $G_R = (\mathcal{V}_R, \mathcal{A}_R)$ with a set of vertices $v \in \mathcal{V}_R$ and a set of road segment arcs $(v, w) \in \mathcal{A}_R$. Each arc $(v, w) \in \mathcal{A}_R$ is characterized by a distance $d_{v,w}$, a traversal time $t_{v,w}$, and energy consumption $c_{v,w}$.

We consider a set $\mathcal{T} = 1, \ldots, T$ of discrete equidistant time steps (each of duration $\Delta t \in \mathbb{R}^+$) and a set $\mathcal{C} = \{1, \ldots, C\}$ of equidistant discrete battery charge levels (each has energy $E_c \in \mathbb{R}^+$).

While some vertices in G_R merely represent intersections or access points, others represent charging stations $\mathcal{S} \subseteq \mathcal{V}_R$ that allow recharging of vehicles. Each charging station $s \in \mathcal{S}$ has a charging rate $\delta_{C,s} \in \{1, \ldots, C\}$ that denotes the amount of SoC that can be recharged in a single time step. Additionally, charging stations have a certain number of charging plugs $\bar{S}_s \in \mathbb{N}^+$, which limits the number of concurrently charging vehicles.

We model congestion using a threshold model, i.e., we assume that vehicles drive at the road's free-flow speed as long as their number is less than the road's capacity $\bar{f}_{v,w} \in \mathbb{R}^+$, as detailed in [20].

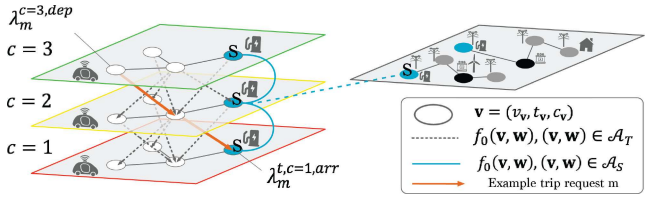

Fig. 1. Integration of an expanded road graph (left) and multiple power distribution networks (PDNs) (right). Typically, a road network spans across multiple PDNs and connects to the PDNs via charging station vertices. Besides charging stations that represent controllable loads, PDNs contain reference buses (typically substations) highlighted in black and uncontrollable loads from residential and commercial customers.

B. Expanded Graph Representation

We use an expanded graph to model a vehicle's location and SoC over time. The expanded graph $G = (\boldsymbol{\mathcal{V}}, \mathcal{A})$ is directed and has a vertex set $\boldsymbol{\mathcal{V}} \subseteq \mathcal{V}_R \times \mathcal{T} \times \mathcal{C}$. Each vertex $\mathbf{v} \in \boldsymbol{\mathcal{V}}$ is defined by a tuple $(v_\mathbf{v}, t_\mathbf{v}, c_\mathbf{v})$ that represents a vertex $v_\mathbf{v}$ of $\mathcal{V}_R$ at a specific time $t_\mathbf{v}$ with a specific SoC $c_\mathbf{v}$. Fig. 1 (left) illustrates the concept of SoC expansion; for ease of representation, the time expansion is not shown. The resulting arc set $\mathcal{A}$ consists of two subsets $\mathcal{A}_T \cup \mathcal{A}_S = \mathcal{A}$. Arcs $(\mathbf{v}, \mathbf{w}) \in \mathcal{A}_T$ represent travel in the road network and must meet the following condition:

$$\mathcal{A}_T = \{(\mathbf{v}, \mathbf{w}) \in \mathcal{A} \mid (v_\mathbf{v}, v_\mathbf{w}) \in \mathcal{A}_R, \; t_\mathbf{w} - t_\mathbf{v} = t_{v_\mathbf{v}, v_\mathbf{w}}, \; c_\mathbf{v} - c_\mathbf{w} = c_{v_\mathbf{v}, v_\mathbf{w}}\}$$

that is: 1) $(v_\mathbf{v}, v_\mathbf{w})$ is a road arc; 2) the time expansion $t_\mathbf{w} - t_\mathbf{v}$ equals its traversal time $t_{v_\mathbf{v}, v_\mathbf{w}}$; and 3) the SoC expansion $c_\mathbf{w} - c_\mathbf{v}$ equals its consumption $c_{v_\mathbf{v}, v_\mathbf{w}}$. Arcs $(\mathbf{v}, \mathbf{w}) \in \mathcal{A}_S$ represent recharging at a charging station and must meet the following condition:

$$\mathcal{A}_S = \{(\mathbf{v}, \mathbf{w}) \in \mathcal{A} \mid v_\mathbf{v} = v_\mathbf{w} = s \in \mathcal{S}, c_\mathbf{w} - c_\mathbf{v} = (t_\mathbf{w} - t_\mathbf{v})\delta_{C,s}\}$$

that is: 1) $v_\mathbf{v}$ and $v_\mathbf{w}$ are equal and correspond to a charging station and 2) the SoC difference $c_\mathbf{w} - c_\mathbf{v}$ equals the amount of energy recharged, that is $(t_\mathbf{w} - t_\mathbf{v})\delta_{C,s}$.

C. Customer Trip Requests

In addition to this graph representation, we define a set of customer trip requests $\mathcal{M} = \{1, \ldots, M\}$. Each trip $m \in \mathcal{M}$ is defined by a quadruple $(v_m, w_m, t_m, \lambda_m) \in \mathcal{V}_R \times \mathcal{V}_R \times \mathcal{T} \times \mathbb{R}^+$ that denotes its origin v_m, its destination w_m, its departure time step t_m, and the number of customer trip requests (i.e.,

the number of customers who wish to travel between v_m and w_m departing at t_m) λ_m. We assume a deterministic setting, in which these requests are known or predicted for all time steps. To reduce the number of decision variables, we use precomputed vehicle routes for customer-carrying vehicles, corresponding to shortest time paths $r_{v\to w}$ that do not violate the congestion constraints. As we use a threshold congestion model, we can straightforwardly precompute such feasible shortest time paths by solving a network flow problem as in [20]. Each shortest time path has a traveling time $t_{v\to w}$ and a charge requirement $c_{v\to w}$. We denote $\lambda_m^{c,\mathrm{dep}}$ as the number of vehicles with charge c departing to serve customer trip request m and $\lambda_m^{t,c,\mathrm{arr}}$ as the as number of vehicles with charge c arriving at time t after serving customer trip request m. Thus, we have

$$\lambda_m^{t,c,\mathrm{arr}} = \begin{cases} \lambda_m^{c+c_{v_m\to w_m},\mathrm{dep}}, & \text{if } t_m = t - t_{v_m\to w_m} \\ 0, & \text{otherwise} \end{cases} \quad \forall t\in\mathcal{T},\ c\in\mathcal{C},\ \forall m\in\mathcal{M}. \tag{1}$$

D. Electric AMoD Model

We introduce $f_0(\mathbf{v},\mathbf{w}) : \mathcal{A}\to\mathbb{R}^+$ to represent the flow of customer-empty vehicles on arc $(\mathbf{v},\mathbf{w})$, which includes both rebalancing and charging vehicles. Furthermore, $N_I(\mathbf{v})$ denotes the initial location of the vehicles, i.e., the number of vehicles available at vertex $v_\mathbf{v}$ with charge level $c_\mathbf{v}$ at $t_\mathbf{v}=1$ and is zero for all other time steps. Analogously, $N_F(\mathbf{v})$ denotes the desired final location of the vehicles, i.e., the number of vehicles that must be at node $v_\mathbf{v}$ with charge level $c_\mathbf{v}$ at $t_\mathbf{v}=T$. With this notation, a multicommodity flow representation of the electric AMoD model is given by

$$\begin{aligned} &\sum_{\mathbf{w}:(\mathbf{v},\mathbf{w})\in\mathcal{A}} f_0(\mathbf{v},\mathbf{w}) + \sum_{m=1}^{M} \mathbb{1}_{v_\mathbf{v}=v_m}\mathbb{1}_{t_\mathbf{v}=t_m}\lambda_m^{c_\mathbf{v},\mathrm{dep}} + N_F(\mathbf{v}) \\ &= \sum_{\mathbf{u}:(\mathbf{u},\mathbf{v})\in\mathcal{A}} f_0(\mathbf{u},\mathbf{v}) + \sum_{m=1}^{M} \mathbb{1}_{v_\mathbf{v}=w_m}\lambda_m^{t_\mathbf{v},c_\mathbf{v},\mathrm{arr}} + N_I(\mathbf{v}) \\ &\forall \mathbf{v}\in\boldsymbol{\mathcal{V}} \end{aligned} \tag{2}$$

$$\sum_{c=1}^{C}\lambda_m^{c,\mathrm{dep}} = \lambda_m\ \forall m\in\mathcal{M}, \qquad \sum_{t=1}^{T}\sum_{c=1}^{C}\lambda_m^{t,c,\mathrm{arr}} = \lambda_m\ \forall m\in\mathcal{M}. \tag{3}$$

Here, $\mathbb{1}_x$ is the indicator function. Equation (2) secures flow conservation for rebalancing and charging vehicles, ensures a sufficient number of empty vehicles in each vertex to cover originating trip requests, and enforces initial and final conditions on the vehicle locations through N_I and N_F. Equation (3) distributes the demand for a given trip request m to vehicles with different SoCs and accumulates vehicles arriving at different times with different SoCs for request m.

E. Electric AMoD Problem

We now extend the basic constraints of the electric AMoD model to a full electric AMoD model. Specifically, we optimize the vehicles' rebalancing routes and charging schedules in order to minimize the cost of operating the electric AMoD system, that is,

$$\begin{aligned} \underset{\substack{f_0,[\lambda_m^{c,\mathrm{dep}}]_{c\in\mathcal{C}},\\ [\lambda_m^{t,c,\mathrm{arr}}]_{c\in\mathcal{C},t\in\mathcal{T}},N_I,N_F}}{\text{minimize}} \quad & V_D \sum_{(\mathbf{v},\mathbf{w})\in\mathcal{A}_T} d_{v_\mathbf{v},v_\mathbf{w}} f_0(\mathbf{v},\mathbf{w}) \\ & + \sum_{(\mathbf{v},\mathbf{w})\in\mathcal{A}_S: v_\mathbf{v}=v_\mathbf{w}=s} V_{\mathrm{el},s}[t_\mathbf{v}]\delta_{C,s} f_0(\mathbf{v},\mathbf{w}) \end{aligned} \tag{4a}$$

subject to

(1)–(3) electric AMoD model

$$\sum_{\substack{(\mathbf{v},\mathbf{w})\in\mathcal{A}_T:\\ v_\mathbf{v}=v,v_\mathbf{w}=w,t_\mathbf{v}=t}} f_0(\mathbf{v},\mathbf{w}) \le \bar{f}_{(v,w),t} \quad \forall (v,w)\in\mathcal{A}_R,\ t\in\mathcal{T} \tag{4b}$$

$$\sum_{\substack{(\mathbf{v},\mathbf{w})\in\mathcal{A}_S:\\ v_\mathbf{v}=v_\mathbf{w}=s,t_\mathbf{v}=t}} f_0(\mathbf{v},\mathbf{w}) \le \bar{S}_s \quad \forall s\in\mathcal{S},\ t\in\mathcal{T} \tag{4c}$$

$$g_I(N_I)=0, \qquad g_F(N_F)=0. \tag{4d}$$

Here, we use the previously introduced concept of expanded graph vertices: each vertex $\mathbf{v}\in\boldsymbol{\mathcal{V}}$ is defined by a tuple $(v_\mathbf{v},\ t_\mathbf{v},\ c_\mathbf{v})\in\mathcal{V}_R\times\mathcal{T}\times\mathcal{C}$. The objective function [see (4a)] minimizes the operational cost of the electric AMoD system, considering time-invariant operational cost per unit distance (e.g., discounted cost for maintenance, tires, and depreciation) $V_D\in\mathbb{R}$ for rebalancing vehicles and time-varying electricity costs $V_{\mathrm{el},s}\in\mathbb{R}$ for recharging vehicles at a charging station $s\in\mathcal{S}$. Fig. 1 depicts example arcs that model such rebalancing and charging flows (f_0), as well as $\lambda_m^{c,\mathrm{dep}}$ and $\lambda_m^{t,c,\mathrm{arr}}$ for an example trip m marked with bold arrows. Equations (1)–(3) impose general flow conservation, while (4b) applies the threshold congestion model to rebalancing flows. As customer-carrying flows are fixed, we do not consider these directly in (4b). Instead, we use the residual road capacity $\bar{f}_{(v,w),t}$, which results from subtracting the customer carrying flow on road arc (v,w) at time step t from the corresponding road capacity $\bar{f}_{v,w}$. The prerouted vehicles may congest a road link. In this case, we set the residual capacity $\bar{f}_{(v,w),t}$ for that link to zero. Thus, customer-carrying flows and residual capacity are fixed and constant with respect to the optimization of rebalancing flows. Equation (4c) limits the number of vehicles that can use a charging station concurrently according to the number of charging plugs at each station. We impose initial and final conditions on vehicles with the generic functions g_I and g_F in (4d). The brackets in the decision variables denote concatenation. We will use this convention in the rest of this article.

The electric AMoD problem [see (4)] has $TC(|\mathcal{A}_R|+|\mathcal{S}|)+CM+TC|\mathcal{V}_R|+C|\mathcal{V}_R|$ decision variables. The dominant term is CM: there could be at most one customer trip request from every origin to every destination at every time step such that $M\le|\mathcal{V}_R|^2T$. It follows that $CM\in\mathcal{O}(C|\mathcal{V}_R|^2T)$.

A few comments are in order. First, we consider discrete-time steps as well as discrete SoC levels. From a mesoscopic viewpoint, these discretizations bear sufficient accuracy while

improving the model's computational tractability significantly. Second, the network flow model treats vehicles and customers as fractional flows; accordingly, it is not readily suitable for real-time control of electric AMoD fleets. Again, this accuracy loss is acceptable at a mesoscopic level and is compatible with our goal of assessing the achievable performance stemming from the coordination between electric AMoD and PDN operators. Note that our solution can still be used as a reference plan for a lower level microscopic controller (cf.[25]). Third, we limit the vehicle flow on a given road link to its capacity and assume vehicles travel at free-flow speed accordingly. Such a threshold congestion model is in line with the accuracy requirements of our mesoscopic viewpoint. If necessary, more sophisticated congestion models can easily be integrated into our modeling approach, at the cost of computational tractability. Fourth, our model does not explicitly account for congestion from non-AMoD traffic. However, this type of traffic can be considered by subtracting the corresponding flow from the residual road capacity $\bar{f}_{(v,w),t}$. Fifth, we assume that future trip requests are known or estimated with a high degree of accuracy. While the development of tools to estimate AMoD demand is beyond the scope of this article, remarkably accurate algorithms are available in the literature (e.g.,[26]). Sixth, we optimize only rebalancing trips and fix customer trips to their shortest time paths. In principle, including the optimization of customer-carrying trips could yield solutions with lower cost; however, our prior work has shown that the inclusion of customer-carrying trips in the optimization problem results in a small decrease in cost at the price of a significant increase in computational complexity [20]. Also note that although the route of customer-carrying trips is fixed, the SoC of customer-carrying vehicles is part of the optimization problem. Finally, the electric AMoD problem [see (4)] may become infeasible if the number or the distribution of customer trip requests exceeds the customer-carrying capacity of the electric AMoD system. Here, we assume that the problem is always feasible as the fleet operator can reject or postpone trip requests to ensure feasibility. This is in line with common practice in today's taxi or ride-hailing platforms. Nonetheless, a mechanism to decide which trips should be rejected or postponed is beyond the scope of this article.

III. Modeling Unbalanced PDNs

This section provides the basics for modeling unbalanced PDNs and presents the identification of a compatible convex power flow surrogate to model the integration of PDN into an electric AMoD model under a unified notation framework. First, we introduce an unbalanced PDN model in Section III-A. Then, we define the OPF problem in Section III-B. Finally, we compare convex power flow surrogates in Section III-C and justify the selected surrogate.

A. Unbalanced PDN Model

In the following, we consider only the radial network structure that is the typical configuration for PDNs [23, Ch. 1.1] and base our notation on [22]. A radial PDN is modeled as a directed graph $P = (\mathcal{N}, \mathcal{E})$ with a tree topology, consisting of a set of buses $\mathcal{N} = \{0, \dots, N\}$ and a set of links $\mathcal{E} \subset \mathcal{N}^2$.

Each PDN has a reference bus, which typically denotes a substation that connects the PDN to the transmission network. The set $\mathcal{N}^+ = \mathcal{N} \setminus 0$ contains all buses other than the reference bus 0. Buses are connected by links (e.g., power lines, transformers, and regulators), such that $(n, o) \in \mathcal{E}$ represents a link between n and o for which n lies in the single path between the reference bus 0 and bus o. Note that there is only one such path because, by assumption, P is a tree.

We consider unbalanced PDNs with three phases $\Phi = \{a, b, c\}$. In line with this, $\Phi_{n,o} \subseteq \Phi$ is the set of phases in link $(n, o) \in \mathcal{E}$. Furthermore, the set of phases in bus $n \in \mathcal{N}$ comprises the phases of all links connected to the bus

$$\Phi_n = \left(\cup_{(m,n)\in\mathcal{E}} \Phi_{m,n}\right) \cup \left(\cup_{(n,o)\in\mathcal{E}} \Phi_{n,o}\right) \quad \forall n \in \mathcal{N}.$$

Each bus n has a time-invariant shunt admittance matrix $\boldsymbol{Y}_n \in \mathbb{C}^{|\Phi_n|\times|\Phi_n|}$, representing the admittance between the bus and the ground. Furthermore, each link (n, o) has a time-invariant impedance matrix $\boldsymbol{Z}_{n,o} \in \mathbb{C}^{|\Phi_{n,o}|\times|\Phi_{n,o}|}$.

We consider a discrete-time model that tracks a series of steady states in the power network and neglects dynamic effects. This is appropriate if the discretization time is substantially longer than the time scale for the dynamic effects (i.e., in the order of minutes). We consider a time span $\mathcal{T} = \{1, \dots, T\}$ with time steps $t \in \mathcal{T}$, each having a length $\Delta t \in \mathbb{R}^+$. Each bus n has a time-dependent complex voltage $v_n^\phi[t] \in \mathbb{C}$ and a complex power injection $s_{\text{inj},n}^\phi[t] \in \mathbb{C}$ for each of its phases. Concurrently, each link shows a time-dependent current for each of its phases $i_{n,o}^\phi[t] \in \mathbb{C}$. For brevity, we use vectors for per-phase quantities: $\boldsymbol{v}_n = [v_n^\phi]_{\phi\in\Phi_n}$, $\boldsymbol{s}_{\text{inj},n} = [s_{\text{inj},n}^\phi]_{\phi\in\Phi_n}$, and $\boldsymbol{i}_{n,o} = [i_{n,o}^\phi]_{\phi\in\Phi_{n,o}}$. Herein, superscripts represent the projection onto specific phases.

The current on each link obeys Ohm's law, i.e.,

$$i_{n,o}^\phi[t] = \boldsymbol{Y}_{n,o}((\boldsymbol{v}_n[t])^{\Phi_{n,o}} - (\boldsymbol{v}_o[t])^{\Phi_{n,o}}) \quad (n,o) \in \mathcal{E},\, t \in \mathcal{T}$$

with $\boldsymbol{Y}_{n,o} = \boldsymbol{Z}_{n,o}^{-1}$ [22]. Each bus is either specified by its voltage or by its power injection such that the remaining quantity is a dependent variable [27, Ch. 6.4]. We refer to specified variables as *direct variables* and to those that are dependent as *indirect variables*. The reference bus specifies the reference voltage $v_{\text{ref}}^\phi[t] \in \mathbb{R}$ for the network

$$v_0^\phi[t] = v_{\text{ref}}^\phi[t] \quad \phi \in \Phi_0,\, t \in \mathcal{T}. \tag{5}$$

Accordingly, the complex voltage $\boldsymbol{v}_0$ is the direct variable and the complex power injection $\boldsymbol{s}_{\text{inj},0}$ remains dependent.

For all other buses $n \in \mathcal{N}^+$, the complex power injection $\boldsymbol{s}_{\text{inj},n}$ is the direct variable, whereas the complex voltage $\boldsymbol{v}_n$ remains dependent. These buses are called PQ buses since the active (p) and reactive power injection (q) are the direct variables. Herein, each PQ bus has a time-varying uncontrollable load with complex power $\boldsymbol{s}_{\text{unc},n}[t] \in \mathbb{C}^{|\Phi_n|}$. These loads represent electricity demand from residential and commercial customers. We consider uncontrollable loads to be exogenous but known in advance within time span $\mathcal{T}$.

Controllable loads $\ell \in \mathcal{L} = \{1, \ldots, L\}$ are defined by a tuple $(\boldsymbol{s}_{\text{con},\ell}[t], n_\ell) \in \mathbb{C}^{|\Phi_{n_\ell}|} \times \mathcal{N}$ denoting their complex power $\boldsymbol{s}_{\text{con},\ell}$ and its corresponding bus n_ℓ. These loads represent dispatchable generators or loads that can be throttled. With this notation, the power injections at PQ buses are

$$\boldsymbol{s}_{\text{inj},n}[t] = -\boldsymbol{s}_{\text{unc},n}[t] - \sum_{\ell=1}^{L} \mathbb{1}_{n=n_\ell} \boldsymbol{s}_{\text{con},\ell}[t] \;\; n \in \mathcal{N}^+, t \in \mathcal{T}. \tag{6}$$

Note that we model generators as negative loads without loss of generality. Furthermore, we consider only wye-connected constant power loads, which may require performing delta-to-wye conversions for some loads and approximating constant current and constant impedance loads as constant power ones. This simplification is common in optimization frameworks [28].

Dependent variables result from the network topology and its controllable and uncontrollable loads. Specifically, they are related by the power flow equation [29]

$$\begin{aligned} \boldsymbol{s}_{\text{inj},n}[t] = \; & \operatorname{diag}(\boldsymbol{v}_n[t]\boldsymbol{v}_n[t]^H \boldsymbol{Y}_n^H) \\ & + \sum_{n:(n,o)\in\mathcal{E}} \operatorname{diag}(\boldsymbol{v}_n{}^{\Phi_{n,o}}[t](\boldsymbol{v}_n{}^{\Phi_{n,o}}[t] \\ & - v_o^{\Phi_{n,o}}[t])^H \boldsymbol{Y}_{n,o}^H)^{\Phi_n}, \quad t \in \mathcal{T}. \end{aligned} \tag{7}$$

Collectively, these equations allow us to model a radial time-invariant unbalanced PDN with time-varying controllable and uncontrollable loads.

A few comments are in order. First, we consider a discrete-time model that tracks a series of steady states in the power network. As we are not interested in dynamic effects, this model is appropriate, and the level of aggregation is aligned with our mesoscopic transportation model. Second, we consider a time-invariant PDN, which cannot model control elements, e.g., step voltage regulators. Optimization frameworks commonly neglect these elements (see [24] and [29]) as their inclusion substantially increases complexity, while their omission results in a more conservative optimization. This simplification is appropriate for the purposes of a mesoscopic system-level analysis. Third, we assume that high-quality estimates of uncontrollable electrical loads are available. While deriving such estimates exceeds our scope, techniques to accurately estimate future power demand exist (see, e.g.,[30]).

B. OPF Problem

The OPF problem [see (8)] optimizes a power network's state subject to its operational constraints and is often used to support grid-related decisions, e.g., operational or strategic planning, and pricing [31]. Here, we use an OPF problem for operational planning and decide on the controllable loads while optimizing a generic objective function $f(\cdot)$ subject to the power flow equation [see (7)] and additional operational constraints:

$$\underset{[[\boldsymbol{v}_n]_{n\in\mathcal{N}}, \boldsymbol{s}_0, [\boldsymbol{s}_{\text{con},\ell}]_{\ell\in\mathcal{L}}]_{t\in\mathcal{T}}}{\text{minimize}} \quad f(\cdot) \tag{8a}$$

subject to

(5) Voltage at reference bus

(6) Power injections

(7) Power flow equation

$$|v_n^\phi[t]| \geq u_{\min,n}^\phi \quad \phi \in \Phi_n, n \in \mathcal{N}^+, t \in \mathcal{T} \tag{8b}$$

$$|v_n^\phi[t]| \leq u_{\max,n}^\phi \quad \phi \in \Phi_n, n \in \mathcal{N}^+, t \in \mathcal{T} \tag{8c}$$

$$\left| \sum_{\phi \in \Phi} s_0{}^\phi[t] \right| \leq \hat{s}_0 \quad t \in \mathcal{T} \tag{8d}$$

$$p_{\text{con},\min,\ell}^\phi \leq p_{\text{con},\ell}^\phi[t] \leq p_{\text{con},\max,\ell}^\phi \quad \phi \in \Phi_{n_\ell},\, \ell \in \mathcal{L},\, t \in \mathcal{T} \tag{8e}$$

$$q_{\text{con},\min,\ell}^\phi \leq q_{\text{con},\ell}^\phi[t] \leq q_{\text{con},\max,\ell}^\phi \quad \phi \in \Phi_{n_\ell},\, \ell \in \mathcal{L},\, t \in \mathcal{T}. \tag{8f}$$

Equations (5)–(7) denote the general power network model. Equations (8b) and (8c) constrain the voltage magnitude $|v_n^\phi[t]|$ to be within a minimal $u_{\min,n}^\phi \in \mathbb{R}$ and a maximal $u_{\max,n}^\phi \in \mathbb{R}$ value, according to regulations (e.g., ANSI C84.1). Equation (8d) limits the apparent power injected to the reference bus to be less than $\hat{s}_0 \in \mathbb{R}^+$, typically, to respect the rating of the substation transformer. Equations (8e) and (8f) model the characteristics of controllable loads through lower and upper bounds on active power ($p_{\text{con},\min,\ell}^\phi$, $p_{\text{con},\max,\ell}^\phi \in \mathbb{R}$), and reactive power ($q_{\text{con},\min,\ell}^\phi$, $q_{\text{con},\max,\ell}^\phi \in \mathbb{R}$). The AMoD-OPF joint problem described in Section IV-C will leverage approximations of the operational constraints in (8) and include an electricity cost objective term.

This OPF problem is nonconvex because of 1) the power flow equation [see (7)] and 2) lower bound constraints on voltage magnitudes [see (8b)]. Even the optimization of a balanced single-phase approximation of this problem remains an NP-hard problem [32].

C. Convex Power Flow Surrogates

We desire the joint AMoD-OPF problem to be convex and ideally linear to preserve computational tractability.

Hence, we convexify the OPF problem [see (8)] using a power flow surrogate that approximates the power flow equation [see (7)] with a convex proxy, making the problem formulation computationally tractable. Using such a power flow surrogate, we lose exact knowledge of the indirect variables.

Given the high relevance of the OPF problem, a vast literature on power flow surrogates exists [31], [33]. However, most of these surrogates, as well as comparative studies, consider only balanced single-phase models as typically used in transmission networks [34].

For unbalanced three-phase models, only a few power flow surrogates exist, and, to the best of our knowledge, no survey or benchmark classifies the suitability of these surrogates for specific problem structures, such as integration with the electric AMoD problem. To close this gap, we analyzed and compared three promising surrogates.

We compared a convex, semidefinite program (SDP) surrogate [22], the branch flow model SDP (BFM-SDP), against two linear surrogates: the branch flow model linear program (BFM-LP) [22], [35] and the linearized power flow manifold linear

program (LPFM-LP) [36]. We used the charger maximization problem, which maximizes the power delivered to a series of charging stations across a distribution network as a benchmark, as it challenges the surrogates by pushing the network's operational constraints to its limits. For each surrogate, we evaluated its accuracy in approximating the indirect variables used in (8b)–(8d). Additionally, we analyzed the resulting constraint violations and computational times We detail the methodology of our comparison in [37] but omit it in this article due to space limitations. In summary, BFM-SDP yielded exact solutions on small instances but performed significantly worse than the other two approaches in both solution quality and computational time for large instances. LPFM-LP and BFM-LP showed a tradeoff between solution quality and computational time, with a 91% reduction on the mean average error in approximating bus voltage magnitudes (LPFM-LP) and 97.3% shorter computational times (BFM-LP), while neither of both violated the substation rating constraint. Based on these results, we use the BFM-LP in this work as it preserves linearity in the joint problem while yielding sufficient solution quality for our mesoscopic study and relatively short computation times.

The BFM-LP assumes fixed link losses and fixed voltage ratios between phases in a bus [22], [35]: let $\tilde{\boldsymbol{i}}_{n,o} \in \mathbb{C}^{|\Phi_{n,o}|}$ be the fixed link current in link $(n,o) \in \mathcal{E}$ used to determine the fixed link losses. Let $\tilde{\boldsymbol{v}}_n \in \mathbb{C}^{|\Phi_n|}$ be the voltage used to determine the fixed voltage ratios in bus $n \in \mathcal{N}^+$. Then, the matrix of fixed voltage ratios for link $(n,o) \in \mathcal{E}$, $\boldsymbol{\Gamma}_{n,o} \in \mathbb{C}^{|\Phi_{n,o}| \times |\Phi_{n,o}|}$, has entries

$$(\boldsymbol{\Gamma}_{n,o}[t])_{ij} = \frac{((\tilde{\boldsymbol{v}}_n[t])^{\Phi_{n,o}})_i}{((\tilde{\boldsymbol{v}}_n[t])^{\Phi_{n,o}})_j} \quad i,j \in \{1,\dots,|\Phi_{n,o}|\},$$
$$(n,o) \in \mathcal{E},\ t \in \mathcal{T}.$$

We define the following matrices to ease the notation:

$$\boldsymbol{W}_n[t] = \boldsymbol{v}_n[t]\boldsymbol{v}_n[t]^H$$
$$\boldsymbol{\Lambda}_{n,o}[t] = \operatorname{diag}((\boldsymbol{v}_n[t])^{\Phi_{n,o}} \boldsymbol{i}_{n,o}[t]^H)$$
$$\tilde{\boldsymbol{L}}_{n,o}[t] = \tilde{\boldsymbol{i}}_{n,o}[t]^H \tilde{\boldsymbol{i}}_{n,o}[t] \quad (n,o) \in \mathcal{E},\ t \in \mathcal{T}.$$

Assuming fixed link losses and voltage ratios, the power flow equation [see (7)] admits a linear approximation [29]:

$$\sum_{m:(m,n)\in\mathcal{E}} \boldsymbol{\Lambda}_{n,o}[t] - \operatorname{diag}(\boldsymbol{Z}_{m,n}\tilde{\boldsymbol{L}}_{n,o}[t]) - \operatorname{diag}(\boldsymbol{W}_n[t]\boldsymbol{Y}_n^H) + \boldsymbol{s}_{\mathrm{inj},n}[t] = \sum_{o:(n,o)\in\mathcal{E}} (\boldsymbol{\Lambda}_{n,o}[t])^{\Phi_n} \quad n \in \mathcal{N},\ t \in \mathcal{T} \tag{9}$$

$$\boldsymbol{W}_o[t] = (\boldsymbol{W}_n[t])^{\Phi_{n,o}} - (\boldsymbol{\Gamma}_{n,o}[t]\operatorname{diag}(\boldsymbol{\Lambda}_{n,o})\boldsymbol{Z}_{n,o}^H + \boldsymbol{Z}_{n,o}(\boldsymbol{\Gamma}_{n,o}[t]\operatorname{diag}(\boldsymbol{\Lambda}_{n,o}))^H + \boldsymbol{Z}_{n,o}\tilde{\boldsymbol{L}}_{n,o}[t]\boldsymbol{Z}_{n,o}^H \quad (n,o) \in \mathcal{E},\ t \in \mathcal{T}. \tag{10}$$

The constraints on voltage magnitudes then read as

$$\operatorname{diag}((\boldsymbol{W}_n[t])^{\phi}) \geq (u_{\min,n}^{\phi})^2 \ \phi \in \Phi_n, \quad n \in \mathcal{N}^+,\ t \in \mathcal{T} \tag{11}$$

$$\operatorname{diag}((\boldsymbol{W}_n[t])^{\phi}) \leq (u_{\max,n}^{\phi})^2 \ \phi \in \Phi_n, \quad n \in \mathcal{N}^+,\ t \in \mathcal{T}. \tag{12}$$

Now, each nonlinear term in (8) can be replaced with a linear approximation to yield the BFM-LP: 1) the power flow equation [see (7)] with the branch flow model (BFM) linearization [see (9) and (10)] and 2) the voltage magnitude constraints [see (8b) and (8c)] with their linear approximation [see (11) and (12)]. Note that (8d) constrains a complex scalar to lie within a circle of radius $\hat{s}_0$ in the complex plane. This constraint is nonlinear but convex and can be represented as a second-order cone. To obtain a linear program (LP), we approximate the circle with a 12-face regular polygon [38], which covers more than 95% of the circle's area.

The BFM-LP has $T(\sum_{n\in\mathcal{N}}|\Phi_n|^2 + 2\sum_{(n,o)\in\mathcal{E}}|\Phi_{n,o}| + 2|\Phi_0| + 2\sum_{\ell\in\mathcal{L}}|\Phi_{n_\ell}|)$ decision variables. Here, $T\sum_{n\in\mathcal{N}}|\Phi_n|^2$ is the dominant term since, by assumption, P has a tree topology such that $|\mathcal{N}| = |\mathcal{E}| + 1$. Since voltages are complex-valued (i.e., two components per phase) and Φ_n has at most three phases, it follows that $|\Phi_n|^2 \in \mathcal{O}(1)$. Thus, the dominant term grows proportional to the number of buses $|\mathcal{N}|$ and the number of time steps T. In line with this, it admits an upper bound $\mathcal{O}(T|\mathcal{N}|)$.

A few comments are in order. First, we use a linear power flow surrogate, which entails the approximation of indirect variables. We discuss its validity and attenuate potential constraint violations in Section V. Second, by using the BFM-LP surrogate, we treat link losses and voltage ratios as fixed parameters. Previous research has shown that BFM-LP achieves sufficient accuracy even under the assumption of zero link losses and perfectly balanced voltage ratios [22]. Our formulation is even more accurate since we use reasonable estimates for the fixed parameters instead of setting them to zero [35].

IV. Interaction Between an Electric AMoD System and PDNs

In this section, we develop a model for the joint optimization of an electric AMoD system and a series of PDNs. Specifically, as an electric AMoD system usually spans across multiple (disconnected) PDNs, we first introduce the multi-OPF problem, which combines multiple OPF problem instances. Then, we formalize the coupling between the electric AMoD system and the PDNs before we state the joint AMoD-OPF problem.

A. Multi-OPF Problem

The multi-OPF problem couples D instances of the OPF problem and results straightforwardly by extending the constraints for each instance $d \in \mathcal{D} = \{1,\dots,D\}$.

We neglect couplings upstream of PDN substations through the transmission network as this article focuses solely on the interaction between an electric AMoD system and a series of PDNs. Couplings between the electric AMoD system and the power network at the transmission and distribution level occur on very different spatial scales (tens of kilometers versus

hundreds of meters) and result in largely orthogonal effects: specifically, couplings at the transmission level mainly influence bulk electricity prices [20], whereas couplings at the distribution level influence bus voltages and power losses. Accordingly, due to the orthogonal nature of the two couplings, we envision that a nested optimization approach could be used to first address transmission-level couplings through existing algorithms (see, e.g.,[20]) and then optimize distribution-level couplings through the tools proposed in this article.

B. Coupling of the Electric AMoD System and PDNs

The charging stations, which appear as controllable loads in the PDNs, couple the electric AMoD system to the PDNs (see Fig. 1). Formally, this coupling is established by two functions, $\mathcal{M}_{\mathcal{S},\mathcal{A}_S}$ and $\mathcal{M}_{\mathcal{S},\mathcal{L}}$, defined in the following.

The function $\mathcal{M}_{\mathcal{S},\mathcal{A}_S} : \mathcal{S} \times \mathcal{T} \to \mathcal{A}_S$ maps a charging station $s \in \mathcal{S}$ for each time step $t \in \mathcal{T}$ to all arcs in $\mathcal{A}_S$ that represent charging vehicles at this station:

$$\mathcal{M}_{\mathcal{S},\mathcal{A}_S}(s,t)=\{(\mathbf{v},\mathbf{w})\in\mathcal{A}_S \mid v_{\mathbf{v}}=v_{\mathbf{w}}=s,\ c_{\mathbf{v}}<c_{\mathbf{w}}, t_{\mathbf{v}}\le t\le t_{\mathbf{w}}\}.$$

Then, the load at charging station s is given by

$$p_s[t] = E_c \delta_{C,s} \sum_{(\mathbf{v},\mathbf{w})\in\mathcal{M}_{\mathcal{S},\mathcal{A}_S}(s,t)} f_0(\mathbf{v},\mathbf{w}) \qquad s\in\mathcal{S},\ t\in\mathcal{T}. \tag{13}$$

The function $\mathcal{M}_{\mathcal{S},\mathcal{L}} : \mathcal{S} \to (\mathcal{L} \times \mathcal{D})$ maps a charging station $s \in \mathcal{S}$ to the associated controllable load $\ell \in \mathcal{L}$ and distribution network $d \in \mathcal{D}$. It follows that charging station s is attached to bus $n_{\mathcal{M}_{\mathcal{S},\mathcal{L}}(s)}$ in PDN $d_{\mathcal{M}_{\mathcal{S},\mathcal{L}}(s)}$. As we consider three-phase charging stations, we assume equally distributed loads, that is

$$s^a_{\mathrm{con},\mathcal{M}_{\mathcal{S},\mathcal{L}}(s)}[t] = s^b_{\mathrm{con},\mathcal{M}_{\mathcal{S},\mathcal{L}}(s)}[t] = s^c_{\mathrm{con},\mathcal{M}_{\mathcal{S},\mathcal{L}}(s)}[t] = \frac{1}{3}p_s[t] \qquad s\in\mathcal{S},\ t\in\mathcal{T}. \tag{14}$$

Note that we can model inverters that control the load power factor since $q^{\phi}_{\mathrm{con},\mathcal{M}_{\mathcal{S},\mathcal{L}}(s)}$ must not necessarily be zero. Although the charging station load is distributed equally among phases, loads in distribution networks are inherently unbalanced, which requires an unbalanced distribution model [23, Ch. 1.3] Also note that charging stations are commonly modeled to operate at unity power factor (no reactive power consumption) [39].

C. AMoD-OPF Problem

The joint AMoD-OPF problem results from coupling the electric AMoD problem (4) with the multi-OPF problem through (13) and (14), namely:

$$\begin{aligned}\underset{\substack{f_0,[\lambda_m^{c,\mathrm{dep}}]_{c\in\mathcal{C}},\\ [\lambda_m^{t,c,\mathrm{arr}}]_{c\in\mathcal{C},t\in\mathcal{T}},N_I,N_F,\\ [[\boldsymbol{v}_n]_{n\in\mathcal{N}},[i^{\phi}_{n,o}]_{(n,o)\in\mathcal{E}},\\ \boldsymbol{s}_0,[s_{\mathrm{con},\ell}]_{\ell\in\mathcal{L}}]_{t\in\mathcal{T},\,d\in\mathcal{D}}}}{\text{minimize}} \quad & V_D \sum_{(\mathbf{v},\mathbf{w})\in\mathcal{A}} d_{v_{\mathbf{v}},v_{\mathbf{w}}} f_0(\mathbf{v},\mathbf{w}) \\ & + \sum_{t\in\mathcal{T}} \Delta t \sum_{d\in\mathcal{D}} V_{\mathrm{el},d}[t] \sum_{\phi\in\Phi} p^{\phi}_{0,d}[t] \end{aligned} \tag{15a}$$

subject to

(1)–(3) and (4b)–(4d)	Electric AMoD system
$[(5), (6), (9), \text{and } (10)]_{d\in\mathcal{D}}$ and $[(8b)–(8f)]_{d\in\mathcal{D}}$	PDNs
(13) and (14)	Coupling from charging stations.

The objective (15a) captures operating costs for both the electric AMoD fleet and the PDNs since we consider full cooperation between both operators. Analogously to the isolated electric AMoD problem (4a), we consider only rebalancing costs for the AMoD fleet given fixed customer flows. In each distribution network $d \in D$, we account for the electricity cost that results from charging vehicles, uncontrollable loads, and power losses.

Note that our joint problem formulation treats both operators as a single entity, assuming complete information and cooperation. This assumption is in line with our mesoscopic view and scope to estimate the achievable benefits of coordination and cooperation between the two systems. We leave the study of game-theoretical aspects to future work, where we intend to develop pricing and coordination mechanisms to align the goals of the electric AMoD operator and the PDN operators, and to leverage distributed optimization algorithms to compute a solution to the AMoD-OPF problem (15) in a distributed manner. Furthermore, our joint model assumes that the electric AMoD system is the dominant means of electric transportation, which is in line with our system-level perspective [3]. However, the model can readily accommodate other EVs by including their traffic flow as residual capacity in (4b) and their charging as exogeneous loads in (8).

V. Case Study in Orange County, CA

We evaluate the impact of an electric AMoD system on the PDNs and the benefit of optimized joint coordination through a case study in Orange County, CA. Our case study considers commuting trips within the cities of Fountain Valley, Irvine, North Tustin, Orange, Santa Ana, Tustin, and Villa Park. In the following, we detail our data (see Section V-A), outline the experimental design (see Section V-B), and, finally, discuss our results (see Section V-C).

A. Model Parameters

We focus on an 8-h commuting cycle from 5 A.M. to 1 P.M. on July 3, 2015 discretized into 6-min time steps, such that $|\mathcal{T}| = 80$. As we do not consider future grid storage devices, which would charge/discharge over the span of a day, an 8-h horizon is sufficient to model the power system. We chose the time discretization to be close to the traversal time of the shortest road link. As the power system considers hourly prices and excludes transient effects, 6-min time steps are more than sufficient to model PDNs for a mesoscopic analysis. For this period, we model the charging station and transportation networks at a mesoscopic aggregation level that allows a sufficient level of detail to analyze the interaction between an electric AMoD system and the PDNs, and ensures computational tractability.

1) Transportation Network Data: We derive trip demand from Census Tract Flow data from the 2006–2010 American

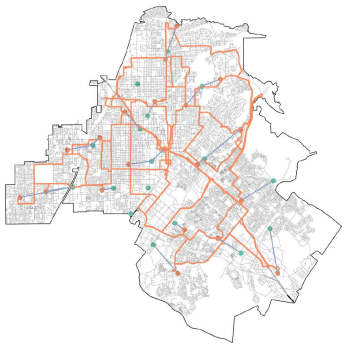

Fig. 2. Area considered in the Orange County, CA case study. The aggregated road network is shown in orange, representing vertices as dots and arcs as lines. Green dots show the substation locations. Blue lines show the assignment of a charging station to its closest substation.

Community Survey. From these data, we take the estimated commuting flows between the 143 census tracts that are part of our case study. To align the granularity of aggregated charging station network representations and census tracts, we cluster the 143 census tracts into 20 larger areas using a k-means algorithm. We neglect commuting flows if they start or end outside the area of our case study or if they start and end within the same cluster since these types of flows cannot be accurately represented in our model. Our planning horizon comprises 122 219 trips (32.8% of the total daily trips).

The problem of fleet sizing for (electric) AMoD systems [40] is beyond the scope of this article. For this case study, we heuristically selected a sufficient fleet size, large enough to keep the AMoD-OPF problem [see (15)] feasible with only a small number of idle vehicles and corresponding to 140% of the peak concurrent number of passenger-carrying trips.

We create an aggregated road network based on OpenStreetMap data with the same granularity as the trip demand data. For this, we select the road network vertices closest to the centroids of the census tract clusters and add arcs between those vertices if a connection exists in the real road network. We obtain an aggregated road network with 20 vertices and 76 arcs (see Fig. 2), which captures vehicle travel and charging between the separate PDNs of the case study region. Note that computational complexity limits our model to coarse road networks; this is discussed in detail below. For each aggregated road network vertex, we consider three-phase 50-kW dc fast-charging stations with $\bar{S}_s = 40$ plugs in total. Accordingly, each vertex has a charging station with a maximum load of 2 MW (0.66 MW per phase).

2) EV Data: We consider a homogeneous vehicle fleet based on the characteristics of the 2018 Nissan Leaf, which has a 40-kWh battery and a range of 240 km. Based on fast-charging guidelines, we reduce a vehicle's battery capacity and its range to 80% of their original values [11] and discretize this effective battery capacity into $C = 40$ levels, resulting in energy discretizations of 0.8 kWh, which remains close to the energy necessary to traverse the lowest energy road link. To account for the possibility that vehicles might not start the day with fully charged batteries, we set the SoC at $t = 1$ to 50%. Furthermore, we require vehicles to recharge the amount of energy used over a planning horizon such that the final SoC must be at a minimum 50% again. We set the vehicle operation cost per unit distance (excluding electricity) to $V_D = 0.3$ USD/km [41].

3) PDN Data: We use a GridLAB-D model of the PL-1 distribution network, a primary feeder operated by the Pacific Gas and Electric Company available for research purposes [42], as a proxy for (sub-)urban distribution networks. The network comprises 322 buses and operates at a nominal voltage of 12.6 kV. We set the uncontrollable loads to the model's time-varying loads.

We take the location of substations from the utility's data [43] and attach a model of the PL-1 distribution network to each substation. We set the electricity price at each substation to the corresponding locational marginal price [44] and conservatively assume a base load utilization of 75% at the substation transformer. Typically, distribution networks are operated at 50–75% of their load capacity so that loads can be transferred from one distribution network to another if needed [45]. Accordingly, we set the substation transformer rating $\hat{s}_0$ to $1/0.75$ times the value of the peak base load (i.e., without charging stations), yielding $\hat{s}_0 = 10.42$ MVA. In addition, we set the lower voltage magnitude limit to 0.96 per unit and the upper limit to 1.04 per unit, which is 0.01 per unit tighter than required by ANSI C84.1 to allow for the voltage drop in the secondaries of the network.

We connect each charging station to the distribution network whose substation is nearest. Since no data on the coordinates of the distribution network buses exist, we randomly attach the charging station to one of the PDN buses. Thus, the PDN is the same for each substation, except for the varying number and location of charging stations. In total, we consider 14 distribution networks, each with one or two charging stations.

We set the price of electricity at each charging station to be equal to the electricity price at the respective substation, such that $V_{\text{el},s}[t] = V_{\text{el},d_{\mathcal{M}_{S,\mathcal{L}}(s)}}[t]$ holds. Since we focus on the total benefit from a system perspective and treat both operators as a single entity, only the spatial variation of electricity prices that are closely linked to the substation prices affects our solution.

Some comments on the distribution network modeling are in order. First, we used the same network model and load values for each distribution network, considering loads from a single summer day. As PDNs are treated as critical infrastructure and load data are usually confidential to protect customers, more accurate data are not publicly available for research purposes [46]. However, our model can be rerun with more accurate data at any time. Second, we set the electricity price at each substation to the corresponding locational marginal price. Locational marginal prices result from the power consumption at the transmission grid level. As our focus is on the interaction of the electric AMoD fleet with the distribution grids and the power used for recharging represents only a negligible fraction at the transmission grid level, neglecting the impact of this consumption on the marginal prices only minimally affects the accuracy of our results. Third,

we assume the electricity price for charging at a certain station to be equal to the electricity price at the respective substation. Neglecting the possible difference in electricity prices among nodes in a single distribution network is consistent with our mesoscopic transportation model.

The resulting AMoD-OPF problem has 6 224 240 decision variables, 1 463 600 from the electric AMoD part and 4 760 640 from the multi-OPF part. Since the multi-OPF part comprises D PDNs, the number of variables in it admits the upper bound $\mathcal{O}(TD|\mathcal{N}|)$. Thus, the number of decision variables in the whole AMoD-OPF problem admits the following upper bound: $\mathcal{O}(T(C|\mathcal{V}_R|^2 + D|\mathcal{N}|))$. Recall that the complexity of solving the LP with an interior point method is polynomial in the number of variables with an exponent lower than 3.5 (depending on the implementation) [47]. Nominally, the size of the electric AMoD part of the problem increases quadratically with the number of road vertices. However, if more vertices are added for the same area, the road segment arcs will become shorter, and T and C should be increased to capture the reduced travel duration and energy consumption in the shorter road segment arcs. Thus, in practice, the electric AMoD part of the problem grows more than quadratically with the number of road vertices. This limits our formulation to coarse road networks. In future work, we will explore methods that improve the scalability of the AMoD-OPF problem, extending its applicability to finer networks.

B. Experimental Design

To quantify the impact of an electric AMoD system on the PDNs and the benefit of optimized joint coordination, our experiments consider two cases. First, we analyze the impact of an electric AMoD system on the PDNs without coordination, i.e., the uncoordinated case. This study shows how electric AMoD systems can negatively affect PDNs. Then, we focus on the coordinated case in which the electric AMoD system and the distribution networks are jointly optimized. Comparing the results of both cases allow us to quantify the potential of optimized coordination between these systems. In both cases, we generate results as follows.

a) Computing controllable loads. We determine the load at each charging station that results from the operation of the electric AMoD system. Depending on the studied case, we solve either (4) (uncoordinated) or (15) (coordinated).

b) Solving the power flow equation. To assess the quality of a solution from step (a), we solve the exact power flow equation [see (7)] to derive the true values of the indirect variables (i.e., complex power injection at the reference bus and complex voltage in all other buses).

c) Evaluating constraint violations. In step (a), we determine controllable loads without an exact model of the PDNs as it is either neglected (uncoordinated case) or approximated (coordinated case). Hence, it is often the case that solutions do violate some of the constraints. To quantify these violations, we evaluate integral constraint violations as we consider a time-variant model. Specifically, regulations require voltage magnitudes to be kept within a given percentage of a nominal value (e.g., ANSI C84.1). Hence, we analyze the integral absolute voltage magnitude constraint violation

$$u_{\text{viol,int}} = \Delta t \sum_{t\in\mathcal{T}} \sum_{d\in\mathcal{D}} \sum_{n\in\mathcal{N}_d^+} \sum_{\phi\in\Phi_{n,d}} |u^{\phi}_{\text{viol},n,d}[t]|$$

where

$$u^{\phi}_{\text{viol},n,d}[t] = \min(u^{\phi}_{n,d}[t] - u^{\phi}_{\min,n,d},\, 0) + \max(u^{\phi}_{n,d}[t] - u^{\phi}_{\max,n,d},\, 0)$$

is the voltage magnitude constraint violation at phase $\phi \in \Phi_n$ in bus $n \in \mathcal{N}$. Note that $u^{\phi}_{\text{viol},n,d}$ is negative when the voltage magnitude is lower than $u^{\phi}_{\min,n,d}$, positive when it is larger than $u^{\phi}_{\max,n,d}$, and zero when it is in-between. Additionally, substations typically connect distribution networks to the higher-voltage transmission network, requiring a transformer to lower the voltage. To avoid overloading this transformer, the power draw must be less than the transformer rating. Hence, we analyze the integral substation transformer rating violation

$$\hat{s}_{0,\text{viol,int}} = \sum_{t\in\mathcal{T}} \Delta t \sum_{d\in\mathcal{D}} \hat{s}_{0,d,\text{viol}}[t]$$

where

$$\hat{s}_{0,d,\text{viol}}[t] = \max\left(\left|\sum_{\phi\in\Phi_{0,d}} {s_{0,d}}^{\phi}[t]\right| - \hat{s}_{0,d},\, 0\right)$$

is the substation transformer rating violation for $d \in \mathcal{D}$.

d) Evaluating energy consumption and cost. We analyze the energy consumption of the electric AMoD system and its cost. The total energy consumption E_{total}, which includes the energy consumed by exogenous loads and the electric AMoD system, results from summing the energy draw of all substations. The total energy consumption in the base case $E_{\text{total,base}}$ results analogously without considering an electric AMoD system. Consequently, the difference of E_{total} and $E_{\text{total,base}}$ represents the additional energy consumption caused by the electric AMoD system:

$$\begin{aligned} E_{\text{AMoD}} &= E_{\text{total}} - E_{\text{total,base}} \\ &= \sum_{t\in\mathcal{T}} \Delta t \sum_{d\in\mathcal{D}} \sum_{\phi\in\Phi_{0,d}} ({p_{0,d}}^{\phi}[t] - p^{\phi}_{base,d}[t]). \end{aligned}$$

Here, $p^{\phi}_{base,d} \in \mathbb{R}$ is the power drawn in phase $\phi \in \Phi_0$ from substation $d \in \mathcal{D}$ in the base case.

Due to losses in the distribution networks, not all of E_{AMoD} relates to charging stations. The energy delivered to the charging stations is given by

$$E_{\text{charge,AMoD}} = \sum_{t\in\mathcal{T}} \Delta t \sum_{d\in\mathcal{D}} \sum_{\ell\in\mathcal{L}_d} \sum_{\phi\in\Phi_{n_\ell,d}} p^{\phi}_{\text{con},\ell,d}[t].$$

The difference between E_{AMoD} and $E_{\text{charge,AMoD}}$ represents the link losses caused by the electric AMoD system:

$$E_{\text{loss,AMoD}} = E_{\text{AMoD}} - E_{\text{charge,AMoD}}.$$

Analogously, the cost of these losses is given by

$$V_{\text{el,loss,AMoD}} = V_{\text{el,AMoD}} - V_{\text{el,charge,AMoD}}$$

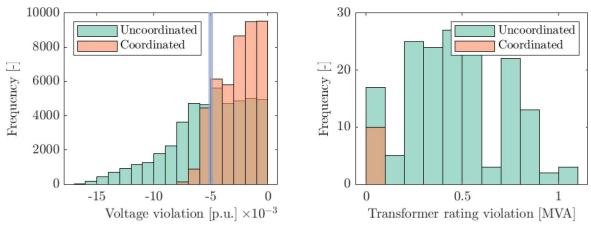

Fig. 3. Histograms of voltage magnitude ($u^{\phi}_{\text{viol},n,d}$) and substation transformer rating ($\hat{s}_{0,d,\text{viol}}$) violations. For clarity, we do not show the cases where the violation is zero. All voltage magnitude violations are negative because the upper limit $u^{\phi}_{\text{max},n,d}$ is never exceeded. The vertical line indicates the threshold for serious voltage magnitude violation events (i.e., those exceeding 0.005 p.u.) For both quantities, constraint violations are significantly lower in the coordinated case. (a) Voltage magnitude. (b) Substation transformer rating.

TABLE I
IMPACT OF COORDINATING AN ELECTRIC AMOD FLEET WITH PDNS

	Unit	Uncoord	Coord	Change
Voltage violation	p.u. h	24.04	11.95	−50.28%
Capacity violation	MVAh	7.89	0.02	−99.71%
Electricity cost, charging	USD	8.35k	8.49k	1.67%
Electricity cost, losses	USD	0.35k	0.33k	−4.59%
Electricity cost, AMoD	USD	8.69k	8.82k	1.42%
Rebalancing cost	USD	97.79k	101.00k	3.28%
Total cost, AMoD	USD	106.49k	109.82k	3.13%
Energy, charging	MWh	268.82	270.63	0.68%
Energy, losses	MWh	11.01	10.43	−5.24%
Energy, AMoD	MWh	279.82	281.06	0.44%

Coordination significantly reduces constraint violations at the cost of slightly higher operational costs.

where $V_{\text{el,AMoD}}$ is given by

$$V_{\text{el,AMoD}} = \sum_{t\in\mathcal{T}} \Delta t \sum_{d\in\mathcal{D}} V_{\text{el},d}[t] \sum_{\phi\in\Phi_{0,d}} ({p_{0,d}}^{\phi}[t] - p^{\phi}_{base,d}[t])$$

and $V_{\text{el,charge,AMoD}}$ is the cost of $E_{\text{charge,AMoD}}$:

$$V_{\text{el,charge,AMoD}} = \sum_{t\in\mathcal{T}} \Delta t \sum_{d\in\mathcal{D}} V_{\text{el},d}[t] \sum_{\ell\in\mathcal{L}_d} \sum_{\phi\in\Phi_{n_\ell,d}} p^{\phi}_{\text{con},\ell,d}[t].$$

Our implementation builds on top of the authors' AMoD Toolkit,[1] which relies on YALMIP [48] to formulate and solve electric AMoD problems. Additionally, we built a general codebase for unbalanced OPF problems, the Unbalanced OPF Toolkit.[2] To support future research in this field, we released both the AMoD Toolkit and the Unbalanced OPF Toolkit under an open-source license.

C. Results and Discussion

Following our experimental design, we evaluate constraint violations (see Fig. 3), as well as energy consumption and costs. Table I summarizes the key results.

Fig. 3(a) shows a histogram with all voltage magnitude constraint violations $u^{\phi}_{\text{viol},n,d}$; each event represents the constraint being violated in one phase during one of the 6-min time steps. The base case shows no violations and, hence, is not plotted. In contrast, violations appear in both cases that include the electric AMoD system. ANSI C84.1, the power quality standard for voltage ranges used across the USA, advises that service voltage violations must be limited in extent, frequency, and duration. Optimized coordination between the electric AMoD system and the PDNs helps to decrease voltage constraint violations significantly. The number of voltage constraint violations is reduced by 3.85% in the coordinated case, from 46 910 to 45 106. Notably, coordination reduces the number of serious violation events [i.e., those exceeding 0.005 p.u., which are the most concerning; see Fig. 3(a)] by 74.85%, from 21 734 to 5 467. All in all, there is a 50.28% reduction in integral absolute voltage magnitude constraint violation, from 24.04 p.u.-hour to 11.95 p.u.-hour. Consequently, coordination between the two systems helps to achieve better compliance with regulations that require the voltage magnitude to be kept close to its nominal value.

Fig. 3(b) shows a histogram with all substation transformer rating violations $\hat{s}_{0,d,\text{viol}}$ each event represents the constraint being violated in one substation transformer during one of the 6-min time steps. Optimized coordination nearly eliminates substation capacity constraint violations, reducing their count by 94.05% from 168 to 10. The number of substations that experience a transformer rating violation is reduced from six to two. All in all, there is a 99.71% reduction in integral substation transformer rating violation, from 7.89 MVA-hour to 0.02 MVA-hour.

Transformers represent a significant investment by utilities. For example, installing a transformer with a rating similar to the one used in this case study ($\hat{s}_0 = 10.42$ MVA) has a cost in the order of 1.7 million USD [49]. Given transformers' substantial cost, increasing their useful life by reducing transformer capacity threshold violations (as done by coordination) can lead to significant monetary savings for utilities. We leave the precise quantification of these savings for future research.

Fig. 4 shows the load at one representative substation along with the applicable transformer rating. The load is shown for the three cases: base, uncoordinated and coordinated. The base case represents the substation load arising from the uncontrollable loads. The other two cases show higher loads due to the recharging vehicles. In the uncoordinated case, there is a significant transformer rating violation between 8 A.M. and 11 A.M. Coordination helps to resolve the violation, as charging loads that exceed the capacity constraint are shifted to later time steps.

Fig. 5 shows the number of charging vehicles and the electricity price over time. The coordinated case shows steady charging activity after 11 A.M. In contrast, charging activities decrease significantly after 11 A.M. in the uncoordinated case. The charging activity mirrors the substation load in Fig. 4, which is higher for the coordinated case in later time steps. The increased charging

[1]https://github.com/StanfordASL/AMoD-toolkit
[2]https://github.com/StanfordASL/unbalanced-opf-toolkit

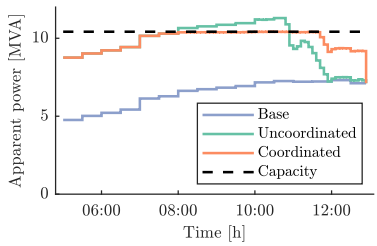

Fig. 4. Load at one representative substation and the corresponding transformer rating. The base case shows the load from uncontrollable loads. The uncoordinated and coordinated cases show increased load due to charging vehicles. The substation transformer rating is exceeded in the uncoordinated case. In the coordinated case, charging vehicles later during the day resolves the violation.

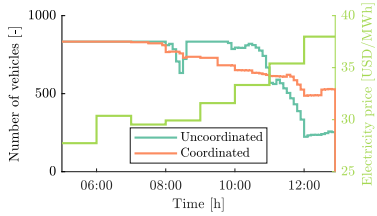

Fig. 5. Number of charging vehicles and electricity price over time. Coordination shifts the charging load to later time steps when the electricity price is higher. The resulting cost increase is the price paid for reducing system constraint violations, which improves voltage profiles and prolongs transformer life.

activity later in the day and the ensuing load leads to increased electricity expenditure as the electricity price is higher later in the day.

Table I shows the impact of coordinating an electric AMoD fleet with PDNs. The total operational costs of the electric AMoD system during the studied 8-h time span increase slightly by 3.13% (3329.61 USD). Rebalancing costs show an increase of 3.28% (3206.47 USD) as vehicles charge at more distant charging stations due to an increase in rebalancing detours. The shift of charging activity to later in the day due to coordination causes electricity costs to increase by 1.42% (123.15 USD). The small increase in operational costs reflects the price paid for reducing system constraint violations, which improves voltage profiles and prolongs transformer life.

The energy delivered to the charging stations (see Table I) increases by 1.82 MWh (0.68%) in the coordinated case because of increased rebalancing detours. However, the energy attributable to the electric AMoD system consumed at the substations increases only by 1.24 MWh (0.44%). The difference of 0.58 MWh is due to energy losses being reduced by 5.24%. Reduced energy losses reflect more efficient power distribution: a greater share of the energy leaving the substations reaches the charging stations in the coordinated case (96.29% compared with 96.07%).

The optimization was performed on an AWS r4.xlarge instance (4 vCPU at 2.3 GHz, 30.5 GB RAM). The AMoD-OPF problem [see (15)] was solved in 554 iterations over 8.1 h, whereas solving the electric AMoD problem [see (4)] took 51 iterations over 0.7 h using Gurobi Optimizer. Thus, the presented solution approach is currently not suitable for real-time operations—the design of an operational version of this framework is left for future research. One potential avenue for reducing the computation time would be improving the scaling of the AMoD-OPF problem [see (15)] to reduce the number of iterations required by the solver. Despite the computation times, the mesoscopic analyses presented herein can be used to identify bottlenecks in PDNs that point at necessary grid extension investments. Additionally, a grid operator can use this approach to compute the amount of spinning reserves needed to hedge on the day-ahead market to secure a reliable operation of its PDNs.

VI. Conclusion

We presented the AMoD-OPF problem, which integrates an electric AMoD problem with a multi-OPF problem. In this context, we discussed power flow surrogates to obtain a computationally tractable convex problem formulation. The resulting AMoD-OPF problem allows one to assess the achievable benefit of coordinating an electric AMoD system and a series of PDNs. With this methodological framework, we investigated the impact of an electric AMoD system on the PDNs. Herein, we especially focused on the benefits of coordination between the two systems and discussed results for a case study in Orange County, CA. We showed that in an uncoordinated system, the electric AMoD fleet negatively affects the distribution networks: the charging behavior of the electric AMoD vehicles caused overloads at substation transformers and violated (lower) voltage magnitude limits. Furthermore, we showed that a coordinated system helps to balance the load in the PDNs in time and space. Specifically, link losses were slightly reduced, substation overloads were nearly eliminated, and voltage violations were halved. Nonetheless, these reductions in constraint violations increased the cost of operating the electric AMoD system by 3.13% caused by vehicles driving to charge in less congested but more distant stations and charging when electricity prices are higher. This indicates that distribution networks can support more EVs before upgrades are needed if the vehicles are charged in coordination with exogenous loads in the PDNs. Due to our system-optimal objective, these findings remain an assessment of the overall benefit of coordination between an electric AMoD fleet and PDNs.

Our findings open the field for multiple directions of future research. First, our AMoD-OPF problem is mesoscopic and assumes perfect knowledge of future loads and trip requests. To design a real-time algorithm, the integration of forecasts to capture the stochastic nature of the problem is an interesting avenue for further research. Second, we modeled the operators of the AMoD fleet and the PDNs as a single entity, implying full cooperation. In future work, one should address the interplay between these two stakeholders, with the goal of designing incentive mechanisms, and investigate market dynamics, e.g., the price of stability and the price of anarchy. Third, our case study provides preliminary results about the benefit of coordinating electric AMoD fleets with PDNs. To provide decision support to practitioners, additional case studies that capture different PDNs, different road network characteristics, varying instance

sizes, and distributed renewable energy generation are required. Fourth, our case study did not consider the EVs' potential to feed power back into the PDN. Hence, extending our modeling approach for vehicle-to-grid options, evaluating regulation and operating reserve potentials, remains a promising avenue for future research.

Acknowledgment

The authors would like to thank Saverio Bolognani, David Chassin, and Raffi Sevlian for sharing their insights on power systems.

References

[1] G. S. Bauer, J. B. Greenblatt, and B. F. Gerke, "Cost, energy, and environmental impact of automated electric taxi fleets in Manhattan," *Environ. Sci. Technol.*, vol. 52, no. 8, pp. 4920–4928, 2018.

[2] K. Spieser, K. Treleaven, R. Zhang, E. Frazzoli, D. Morton, and M. Pavone, "Toward a systematic approach to the design and evaluation of autonomous mobility-on-demand systems: A case study in singapore," in *Road Vehicle Automation*. Berlin, Germany: Springer, 2014, pp. 229–245.

[3] E. Hannon, C. McKerracher, I. Orlandi, and S. Ramkumar, "An Integrated Perspective on the Future of Mobility," McKinsey & Company, Tech. Rep., 2016. [Online]. Available: https://assets.bbhub.io/professional/sites/24/2016/10/BNEF_McKinsey_The-Future-of-Mobility_11-10-16.pdf

[4] H. Shareef, M. M. Islam, and A. Mohamed, "A review of the stage-of-the-art charging technologies, placement methodologies, and impacts of electric vehicles," *Renewable Sustain. Energy Rev.*, vol. 64, pp. 403–420, 2016.

[5] P. Richardson, D. Flynn, and A. Keane, "Optimal charging of electric vehicles in low-voltage distribution systems," *IEEE Trans. Power Syst.*, vol. 27, no. 1, pp. 268–279, Feb. 2012.

[6] K. Clement-Nyns, E. Haesen, and J. Driesen, "The impact of charging plug-in hybrid electric vehicles on a residential distribution grid," *IEEE Trans. Power Syst.*, vol. 25, no. 1, pp. 371–380, Feb. 2010.

[7] M. Pavone, S. L. Smith, E. Frazzoli, and D. Rus, "Robotic load balancing for mobility-on-demand systems," *Int. J. Robot. Res.*, vol. 31, no. 7, pp. 839–854, 2012.

[8] J. Bischoff and M. Maciejewski, "Simulation of city-wide replacement of private cars with autonomous taxis in berlin," *Procedia Comput. Sci.*, vol. 83, pp. 237–244, 2016.

[9] D. J. Fagnant and K. M. Kockelman, "The travel and environmental implications of shared autonomous vehicles, using agent-based model scenarios," *Transp. Res. C: Emerg. Technol.*, vol. 40, pp. 1–13, 2014.

[10] F. Rossi, R. Zhang, Y. Hindy, and M. Pavone, "Routing autonomous vehicles in congested transportation networks: Structural properties and coordination algorithms," *Auton. Robots*, vol. 42, no. 7, pp. 1427–1442, 2018.

[11] D. T. Chen, K. M. Kockelman, and J. P. Hanna, "Operations of a shared, autonomous, electric vehicle fleet: Implications of vehicle & charging infrastructure decisions," *Transp. Res. A: Policy Pract.*, vol. 94, pp. 243–254, 2016.

[12] J. Munkhammar and M. Shepero, "Autonomous electric vehicle fleet charging in cities: Optimal utility estimates and monte carlo simulations," in *Proc. IEEE PES Innov. Smart Grid Technol. Conf.*, 2017, pp. 1–6.

[13] R. Zhang, F. Rossi, and M. Pavone, "Model predictive control of autonomous mobility-on-demand systems," in *Proc. IEEE Conf. Robot. Autom.*, 2016, pp. 1382–1389.

[14] F. Dandl and K. Bogenberger, "Comparing future autonomous electric taxis with an existing free-floating carsharing system," *IEEE Trans. Intell. Transp. Syst.*, vol. 20, no. 6, pp. 2037–2047, Jun. 2019.

[15] S. W. Hadley and A. A. Tsvetkova, "Potential impacts of plug-in hybrid electric vehicles on regional power generation," *Electr. J.*, vol. 22, no. 10, pp. 56–68, 2009.

[16] M. Tran, D. Banister, J. D. K. Bishop, and M. D. McCulloch, "Realizing the electric-vehicle revolution," *Nature Climate Change*, vol. 2, no. 5, pp. 328–333, 2012.

[17] E. Veldman and R. A. Verzijlbergh, "Distribution grid impacts of smart electric vehicle charging from different perspectives," *IEEE Trans. Smart Grid*, vol. 6, no. 1, pp. 333–342, Jan. 2015.

[18] J. J. Q. Yu and A. Y. S. Lam, "Autonomous vehicle logistic system: Joint routing and charging strategy," *IEEE Trans. Intell. Transp. Syst.*, vol. 19, no. 7, pp. 2175–2187, Jul. 2018.

[19] R. Iacobucci, B. McLellan, and T. Tezuka, "Modeling shared autonomous electric vehicles: Potential for transport and power grid integration," *Energy*, vol. 158, pp. 148–163, 2018.

[20] F. Rossi, R. Iglesias, M. Alizadeh, and M. Pavone, "On the interaction between autonomous mobility-on-demand systems and the power network: Models and coordination algorithms," *IEEE Control Netw. Syst.*, vol. 7, no. 1, pp. 384–397, Mar. 2020.

[21] R. Leou, C. Su, and C. Lu, "Stochastic analyses of electric vehicle charging impacts on distribution network," *IEEE Trans. Power Syst.*, vol. 29, no. 3, pp. 1055–1063, May 2014.

[22] L. Gan and S. H. Low, "Convex relaxations and linear approximation for optimal power flow in multiphase radial networks," in *Proc. Power Syst. Comput. Conf.*, 2014, pp. 1–9.

[23] W. H. Kersting, *Distribution System Modelling and Analysis*, 1st ed. Boca Raton, FL, USA: CRC Press, 2002.

[24] J. de Hoog, T. Alpcan, M. Brazil, D. A. Thomas, and I. Mareels, "Optimal charging of electric vehicles taking distribution network constraints into account," *IEEE Trans. Power Syst.*, vol. 30, no. 1, pp. 365–375, Jan. 2015.

[25] R. Iacobucci, B. McLellan, and T. Tezuka, "Optimization of shared autonomous electric vehicles operations with charge scheduling and vehicle-to-grid," *Transp. Res. C: Emerg. Technol.*, vol. 100, pp. 34–52, 2019.

[26] R. Iglesias, F. Rossi, K. Wang, D. Hallac, J. Leskovec, and M. Pavone, "Data-driven model predictive control of autonomous mobility-on-demand systems," in *Proc. IEEE Conf. Robot. Autom.*, 2018, pp. 6019–6025.

[27] J. Glover, M. Sarma, and T. Overbye, *Power System Analysis and Design*, 5th ed. Boston, MA, USA: Cengage Learn., 2011.

[28] A. Bernstein and E. Dall'Anese, "Linear power-flow models in multiphase distribution networks," in *Proc. IEEE PES Innov. Smart Grid Technol. Conf. Eur.*, 2017, pp. 1–6.

[29] C. Zhao, E. Dall'Anese, and S. H. Low, "Optimal power flow in multiphase radial networks with delta connections," in *Proc. IREP Bulk Power Syst. Dyn. Control Symp.*, 2017. [Online]. Available: https://www.osti.gov/biblio/1410967-optimal-power-flow-multiphase-radial-networks-delta-connections-preprint

[30] L. Hernandez *et al.*, "A survey on electric power demand forecasting: Future trends in smart grids, microgrids and smart buildings," *IEEE Commun. Surveys Tuts.*, vol. 16, no. 3, pp. 1460–1495, Jul.–Sep. 2014.

[31] J. A. Taylor, *Convex Optimization of Power Systems*, 1st ed. Cambridge, U.K.: Cambridge Univ. Press, 2015.

[32] J. Lavaei and S. H. Low, "Zero duality gap in optimal power flow problem," *IEEE Trans. Power Syst.*, vol. 27, no. 1, pp. 92–107, Feb. 2012.

[33] D. K. Molzahn and I. A. Hiskens, *A Survey of Relaxations and Approximations of the Power Flow Equations*, 1st ed. Now Foundations and Trends, 2019. [Online]. Available: https://www.nowpublishers.com/article/Details/EES-012

[34] C. Coffrin, D. Gordon, and P. Scott, NESTA, "The NICTA energy system test case archive," 2014, *arXiv:1411.0359*.

[35] M. D. Sankur, R. Dobbe, E. Stewart, D. S. Callaway, and D. B. Arnold, "A linearized power flow model for optimization in unbalanced distribution systems," 2016, *arXiv:1606.04492*.

[36] S. Bolognani and F. Dörfler, "Fast power system analysis via implicit linearization of the power flow manifold," in *Proc. 53rd Annu. Allerton Conf. Commun., Control, Comput.*, 2015, pp. 402–409.

[37] A. Estandia, "On the interaction between autonomous mobility on demand systems and power distribution networks—An optimal power flow approach," Master's Thesis, Dept. Mech. Process, ETH Zurich, Zurich, Switzerland, 2018.

[38] A. Barnes, H. Nagarajan, E. Yamangil, R. Bent, and S. Backhaus, "Tools for improving resilience of electric distribution systems with networked microgrids," 2017, *arXiv:1705.08229*.

[39] M. Kesler, M. C. Kisacikoglu, and L. M. Tolbert, "Vehicle-to-grid reactive power operation using plug-in electric vehicle bidirectional offboard charger," *IEEE Trans. Ind. Electron.*, vol. 61, no. 12, pp. 6778–6784, Dec. 2014.

[40] M. M. Vazifeh, P. Santi, G. Resta, S. H. Strogatz, and C. Ratti, "Addressing the minimum fleet problem in on-demand urban mobility," *Nature*, vol. 557, pp. 534–538, 2018.

[41] Bureau of Transportation Statistics, "National transportation statistics," U.S. Dept. Transp., Washington, DC, USA, Tech. Rep., 2018. [Online]. Available: https://www.bts.gov/sites/bts.dot.gov/files/docs/browse-statistical-products-and-data/national-transportation-statistics/223001/ntsentire2018q4.pdf
[42] Pacific gas and electric company, 2019. [Online]. Available: https://sourceforge.net/p/gridlab-d/code/HEAD/tree/Taxonomy_Feeders/PGE_Models/
[43] Southern CaliforniaEdison, *Substations*, 2019. [Online]. Available: http://data-sce2.opendata.arcgis.com/datasets/7ebd6afdfaeb4d878e141b6b79e9b69f_0
[44] California Independent System Operator. Locational marginal prices (LMP), 2019. [Online]. Available: http://oasis.caiso.com/
[45] K. P. Schneider, Y. Chen, D. P. Chassin, R. Pratt, D. Engel, and S. Thompson, "Modern grid initiative distribution taxonomy final report," Pacific Northwest Nat. Lab., Richland, WA, USA, Tech. Rep. 18035, 2008.
[46] F. E. P. Marcos *et al.*, "A review of power distribution test feeders in the United States and the need for synthetic representative networks," *Energies*, vol. 10, no. 11, 2017, Art. no. 1896.
[47] J. Gondzio, "Interior point methods 25 years later," *Eur. J. Oper. Res.*, vol. 218, no. 3, pp. 587–601, 2012.
[48] J. Löfberg, "YALMIP: A toolbox for modeling and optimization in MATLAB," in *Proc. IEEE Int. Symp. Comput. Aided Control Syst. Des.*, 2014, pp. 284–289.
[49] M. R. Sarker, D. J. Olsen, and M. A. Ortega-Vazquez, "Co-optimization of distribution transformer aging and energy arbitrage using electric vehicles," *IEEE Trans. Smart Grid*, vol. 8, no. 6, pp. 2712–2722, Nov. 2017.

Alvaro Estandia received the B.Sc. degree in mechanical engineering and the M.Sc. degree in robotics from ETH Zurich, Zurich, Switzerland, in 2015 and 2018, respectively.

He is currently a Software Engineer with Marain Inc., Palo Alto, CA, USA. He develops software to simulate and algorithms to control fleets of electrical autonomous vehicles, providing mobility on demand in urban environments. His research interests include applications of optimization for improving the performance of transportation systems and power networks.

Maximilian Schiffer received the Ph.D. degree in operations research from RWTH Aachen University, Aachen, Germany, in 2017.

He is currently an Assistant Professor of operations and supply chain management with the Technical University of Munich, Munich, Germany. His main research interests include operations research, machine learning, and intelligent systems, with an emphasis on transportation and logistics topics, especially electric vehicles and autonomous systems.

Dr. Schiffer is a recipient of the INFORMS TSL Dissertation Prize and the GOR Doctoral Dissertation Prize.

Federico Rossi received the Diploma degree from Alta Scuola Politecnica, Milan, Italy, in 2013, the M.Sc. degree in space engineering from the Politecnico di Milano, Milan, Italy, in 2013, and the Ph.D. degree in aeronautics and astronautics from Stanford University, Stanford, CA, USA, in 2018.

He is currently a Robotics Technologist with the Jet Propulsion Laboratory, California Institute of Technology, Pasadena, CA, USA. His research interests include optimal control and distributed decision making in multiagent robotic systems, with applications to planetary exploration and coordination of fleets of self-driving vehicles for autonomous mobility on demand.

Justin Luke received the B.S. degree in energy engineering from the University of California, Berkeley, CA, USA, in 2018, and the M.S. degree in electrical engineering from Stanford University, Stanford, CA, USA, in 2020. He is currently working towards the Ph.D. degree in civil and environmental engineering at Stanford University, Stanford, CA, USA, in the Autonomous Systems Laboratory and Sustainable Systems Laboratory.

His research interests include optimization methods for integration of electric autonomous mobility-on-demand fleets into the electricity grid, particularly in scenarios with high penetration of renewable generation.

Emre Can Kara received the Ph.D. degree in infrastructure systems, machine learning, and data science from Carnegie Mellon University, Pittsburgh, PA, USA, in 2014.

He is currently leading the engineering and data science efforts with eIQ Mobility, Oakland, CA, USA. His research interests include data-driven methods to integrate HVAC (heating, ventilation, and air conditioning), electric vehicles, and battery storage systems into the electricity grid as flexibility assets.

Ram Rajagopal received the Ph.D. degree in electrical engineering and computer sciences from the University of California, Berkeley, CA, USA, in 2009.

He is currently an Associate Professor of electrical engineering as well as civil and environmental engineering with Stanford University, Stanford, CA, USA, where he directs the Sustainable Systems Laboratory, focused on large-scale monitoring, data analytics, and stochastic control for infrastructure networks, in particular, power networks. His current research interests include integration of renewables, smart distribution systems, and demand-side data analytics.

Marco Pavone received the Ph.D. degree in aeronautics and astronautics from the Massachusetts Institute of Technology, Cambridge, MA, USA, in 2010.

He is currently an Associate Professor of aeronautics and astronautics with Stanford University, Stanford, CA, USA, where he is the Director of the Autonomous Systems Laboratory. His main research interests include development of methodologies for the analysis, design, and control of autonomous systems, with an emphasis on self-driving cars, autonomous aerospace vehicles, and future mobility systems.

Dr. Pavone is an Associate Editor for the *IEEE Control Systems Magazine*.